Orientational cross correlations between entangled branch polymers in primitive chain network simulations

Yuichi Masubuchi, Ankita Pandey, Yoshifumi Amamoto, and Takashi Uneyama

Citation: The Journal of Chemical Physics **147**, 184903 (2017);
View online: https://doi.org/10.1063/1.5001960
View Table of Contents: http://aip.scitation.org/toc/jcp/147/18
Published by the American Institute of Physics

Orientational cross correlations between entangled branch polymers in primitive chain network simulations

Yuichi Masubuchi,[1,a)] Ankita Pandey,[1] Yoshifumi Amamoto,[1] and Takashi Uneyama[2]
[1]*Department of Materials Physics, Nagoya University, Furo-cho, Chikusa-ku, Nagoya 464-8603, Japan*
[2]*Institute of Science and Engineering, Kanazawa University, Kakuma, Kanazawa 920-1192, Japan*

(Received 28 August 2017; accepted 25 October 2017; published online 14 November 2017)

Although it has not been frequently discussed, contributions of the orientational cross-correlation (OCC) between entangled polymers are not negligible in the relaxation modulus. In the present study, OCC contributions were investigated for 4- and 6-arm star-branched and H-branched polymers by means of multi-chain slip-link simulations. Owing to the molecular-level description of the simulation, the segment orientation was traced separately for each molecule as well as each subchain composing the molecules. Then, the OCC was calculated between different molecules and different subchains. The results revealed that the amount of OCC between different molecules is virtually identical to that of linear polymers regardless of the branching structure. The OCC between constituent subchains of the same molecule is significantly smaller than the OCC between different molecules, although its intensity and time-dependent behavior depend on the branching structure as well as the molecular weight. These results lend support to the single-chain models given that the OCC effects are embedded into the stress-optical coefficient, which is independent of the branching structure. *Published by AIP Publishing.* https://doi.org/10.1063/1.5001960

INTRODUCTION

In spite of the remarkable success of the single chain models for entangled polymer dynamics,[1] contributions of the orientational cross-correlation (OCC) among entangled polymers are not negligible. Experimentally, Kornfield and coworkers[2–4] used infrared dichroism and birefringence to report that the OCC contribution accounts for 40% of the relaxation modulus for polystyrene melts. Graf *et al.*[5] reported similar results for polybutadienes by nuclear magnetic resonance (NMR). Molecular simulations also exhibited the effects of the OCC.[6–8] Cao and Likhtman[9] extracted the OCC from the results of molecular dynamics simulations for the bead-spring model to report consistent results with the experiments. In these earlier studies, the origin of the OCC has been discussed in relation to the nematic interactions between Kuhn segments. However, multi-chain slip-link simulations[10–14] have demonstrated that similar OCC contributions are observed even without such explicit two-body interactions. These recent results suggest that the OCC is related to the force balance around entanglement between coupled chains.

The OCC is of importance for further understanding of the relation between polymer dynamics in reality and that assumed in single chain models such as tube[15–18] and slip-link models.[19,20] For linear polymers, Cao and Likhtman[9] have shown that the OCC contribution is insensitive to the molecular weight and the mixing of chains with different molecular weights. Owing to their results, although the OCC contribution is mildly time-dependent, it could be effectively replaced by a numerical prefactor for the stress-optical coefficient of single chain models. Indeed, for some models, the relation between the plateau modulus and entanglement molecular weight does not follow the standard relationship,[21,22] and those two parameters are optimized rather independently to attain reasonable agreements with experiments. However, because the prefactor has been also discussed in relation to the fluctuations at entanglements,[23,24] the OCC contribution should be discriminated from the other effects. It is also noted that the strategy (in which the effects of OCC are embedded into the plateau modulus) may not work for bidisperse systems when the molecular weights and blend ratio for blended chains are highly asymmetric, according to the recent results from the multi-chain slip-link simulations.[12,13]

One of the unexplored problems for the OCC is its contributions in branch polymers. For star-branched polymers, in the framework of tube modeling, the arm chains diverging from the branch point are assumed to move independently with each other, as long as the mean-field description of constraint release is employed.[25,26] However, the arms may possibly move with a correlated manner due to the connectivity at the branch point. For the molecules with multiple branch points such as H-branch polymers, the tube theories are constructed with the assumption so-called hierarchical relaxation,[27–30] in which the backbone chain does not move until the arm chains relax. This picture implicitly assumes a dynamical correlation between the backbone and arm chains. Such correlation may contribute the stress, although it has never been discussed.

In this study, the OCC for 4- and 6-arm star- and H-branch polymers were investigated via multi-chain slip-link

a)Author to whom correspondence should be addressed: mas@nuap.nagoya-u.ac.jp.

simulations. Although the model used here has been known for the lack of thermodynamic rigorousness,[31,32] there is no other practical attack for entangled multi-chain problems at present. For instance, multi-chain slip-spring simulations[33–36] are promising, but the extension to branch polymers has not been attained and it is actually not straightforward for polymers with multiple branch points.

Before the discussion for the OCC, the simulations were validated for the linear viscoelasticity data reported for 4- and 6-arm star-branched and H-branched polystyrene melts in the earlier studies,[37,38] and reasonable agreement with the experimental data was confirmed. Afterwards, the OCC contributions were extracted from the linear relaxation modulus. The results showed that the OCC contribution between different molecules is similar to that for linear polymers being virtually insensitive to the branching structure. The OCC between different constituent chains composing the same molecule is dependent on the molecular weight and the branching structure, reflecting the kinetics of intra-molecular entanglements, though the contribution to the modulus is rather minor. These results lend support to the single chain models, in which the OCC is not explicitly considered, but its effects are embedded into the stress-optical coefficient. Details are given below.

MODEL AND SIMULATION

Because the simulation code used in this study is common with that used in the earlier studies,[39–43] a brief description of the model and the simulation method shall be given here. An entangled polymer system is replaced by a slip-link network, in which each network strand represents a polymer segment having a molecular weight comparable with the entanglement molecular weight. Each polymer chain corresponds to a path through a set of consecutive segments in the network. To restrict the polymer motion perpendicular to its backbone, a slip-link is clipped at each network node.[44] The dynamics of the system is described by the motion of slip-links, sliding motion of polymer chains through the slip-links, and creation/destruction of slip-links around chain ends. The slip-link motion obeys the Langevin-type equation of motion, in which the drag force, balance of tension, osmotic force and Gaussian random force are considered. The polymer sliding is denoted by the rate equation of monomer numbers between two connected segments, according to the common forces with the slip-link dynamics. When a chain end slides out from the slip-link to which the end segment is connected, the slip-link is removed and the coupled chain is released. Vice versa, when an end segment protrudes from the slip-link beyond a certain critical amount, a new slip-link is created on the end segment to hook another surrounding segment randomly. For the case of branch polymers, diffusion of the branch point is considered via the equation of motion identical to that describing the slip-link dynamics.[45] In addition to the diffusion in space, diffusion of the branch point along the backbone is considered to induce the topological change between the branch point and the neighboring slip-links.[41–43,46] When the number of slip-links on the branching arm becomes zero owing to the constraint release of surrounding chains, the branch point (and the branching arm) is allowed to hop across the neighboring slip-link. Although it is rare for the present study under quiescent state, the branch point withdrawal[47] is also implemented. Details of the implemented topological changes around branch points can be found in the earlier publications.[43,46] Nevertheless, the linear and non-linear rheology for various branch polymers has been semi-quantitatively reproduced by the model.

TABLE I. Star-branch polystyrenes.

Code	S-PS1	S-PS2	S-PS3	S-PS4
M_A ($\times 10^3$)	88	256	99	182
q[a]	4	4	6	6
Z_A	8	24	9	17

[a]Number of arms diverging from the branch point.

In the present study, a set of 4- and 6-arm star-branched and H-branched polystyrene melts, for which the linear viscoelastic data are available in the earlier studies,[37,38] was examined. The weight averaged molecular weights of the samples are summarized in Tables I and II. For the star polymers, the molecular weight for each arm M_A is indicated. For the H-polymers, the molecular weights for the arms M_A and the bridging chain between the branch points M_B are listed. A linear polymer melt, for which the data are included in the literature,[37] was also examined for comparison, and its molecular weight is shown as M_B in Table II. In the simulations, the molecular weights of constituent subchains were converted to the number of segments Z according to the unit molecular weight of the model M_0 as $Z = M/M_0$. Note that M_0 is smaller than M_e used for the tube models, owing to the fluctuations imposed on entanglements as reported earlier.[24,40] Nevertheless, as determined for polystyrene melts,[40] M_0 = 11k was used in principle, and then the value of Z was accommodated to attain a reasonable agreement with the experimental data to absorb the effects of polydispersity.[30] The values of Z employed were presented in the tables. The unit modulus G_0 was determined as 0.3 MPa from the value of M_0, the density ρ and the temperature T according to the relation $G_0 = \rho RT/M_0$. Note that the relation between G_0 and M_0 is formally identical to but different from Ferry's relationship between the plateau modulus and entanglement molecular weight. Indeed, G_0 is larger than the plateau modulus. Refer to the earlier publications[24,39,40] for further details of the model parameters. The temperature T was set at T = 169.5 °C, that is, the reference temperature of the experimental data. The unit length a corresponds to the end-to-end distance of the molecule having the molecular weight of M_0, though the value of a is not used explicitly in the simulations. The unit time τ_0 was determined as

TABLE II. H-branch polystyrenes.

Code	H-PS1	H-PS2	H-PS3	L-PS
M_A ($\times 10^3$)	19	44	100	...
M_B ($\times 10^3$)	19	46	103	275
Z_A	2	5	10	...
Z_B	2	5	10	25

$\tau_0 = 3.3 \times 10^{-3}$ s via the fitting of the linear viscoelastic data as shown later.

The simulations were performed with the periodic boundary condition, for which the unit cell dimension was $(10a)^3$. For the osmotic force, the segment density was fixed at 10 and the intensity parameter was $\varepsilon = 1.0$, respectively, unless stated. (See the Appendix for details of the osmotic force.) The correlation functions were obtained from the stress fluctuations recorded during the simulations under quiescent states for sufficiently long time, which is more than 10 times longer than the longest relaxation time. From the stress correlation function, the linear relaxation modulus $G(t)$ was obtained, and $G(t)$ was converted into $G^*(\omega)$ via the fitting to the multi-mode Maxwell function.

CROSS-CORRELATIONS

Following the earlier studies, the segment orientation relaxation function $S(t)$ is defined as

$$S(t) = N_b \left\langle \left(\frac{1}{N_b} \sum_{i=1}^{N_M} M_i^{xy}(t) \right) \left(\frac{1}{N_b} \sum_{i=1}^{N_M} M_i^{xy}(0) \right) \right\rangle. \quad (1)$$

Here, N_b is the total number of segments and N_M is the number of molecules in the system. $\langle \cdots \rangle$ represents the average for the time origin and for the simulations with different initial configurations. $M_i^{xy}(t)$ is the segment orientation for molecule i defined as

$$M_i^{xy}(t) = \sum_j^{N_{Ci}} O_{ij}^{xy}(t). \quad (2)$$

Here, $O_{ij}^{xy}(t)$ and N_{Ci} are the segment orientation and the number of constituent chains for molecule i, respectively. For the star-branched polymers, the sum is taken for all the arms of the molecule, whereas for the H-branched polymers, the sum includes the backbone chain as well as the arms at both sides. For linear polymers, $M_i^{xy}(t)$ is identical to $O_{1,j}^{xy}(t)$.

The segment orientation for the chain $O_{ij}^{xy}(t)$ is written as

$$O_{ij}^{xy}(t) = \frac{n_0}{a^2} \sum_{k=1}^{Z_{ij}} \frac{r_{ijk}^x(t) r_{ijk}^y(t)}{n_{ijk}(t)}. \quad (3)$$

Here, $\mathbf{r}_{ijk}(t)$ and $n_{ijk}(t)$ are the end-to-end vector and the Kuhn-segment number for segment k on chain j in molecule i. These values are normalized by the unit values a and n_0, which are the average values for all the segments. Z_{ij} is the number of segments for chain j in molecule i so that the total segment number N_b in Eq. (1) is written as $N_b = \sum_i^{N_M} \sum_j^{N_{Ci}} Z_{ij}$.

$S(t)$ can be decomposed into the self-correlation for the same molecule $A_M(t)$ and the cross-correlation between different molecules $C_{IM}(t)$ as

$$S(t) = A_M(t) + C_{IM}(t), \quad (4)$$

$$A_M(t) = N_b \frac{1}{{N_b}^2} \sum_i^{N_M} \left\langle M_i^{xy}(t) M_i^{xy}(0) \right\rangle, \quad (5)$$

$$C_{IM}(t) = N_b \frac{1}{{N_b}^2} \sum_{i \neq l}^{N_M} \left\langle M_i^{xy}(t) M_l^{xy}(0) \right\rangle. \quad (6)$$

The self-correlation term in Eq. (4), $A_M(t)$, can be further decomposed into the self-correlation for the same constituent chain $A_C(t)$ and the cross-correlation between different chains (within the same molecule) $C_{IC}(t)$ as

$$A_M(t) = A_C(t) + C_{IC}(t), \quad (7)$$

$$A_C(t) = N_b \frac{1}{{N_b}^2} \sum_i^{N_M} \sum_j^{N_{Ci}} \left\langle O_{ij}^{xy}(t) O_{ij}^{xy}(0) \right\rangle, \quad (8)$$

$$C_{IC}(t) = N_b \frac{1}{{N_b}^2} \sum_i^{N_M} \sum_{j \neq p}^{N_{Ci}} \left\langle O_{ij}^{xy}(t) O_{ip}^{xy}(0) \right\rangle. \quad (9)$$

$A_C(t)$ can be further decomposed into the contributions for the backbone chains and the arm chains for the case of H-branch polymers.

Owing to Eqs. (4) and (7), $S(t)$ can be written as

$$S(t) = A_C(t) + C_{IC}(t) + C_{IM}(t). \quad (10)$$

The coupling parameters are defined from $S(t)$, $C_{IM}(t)$ and $C_{IC}(t)$ as

$$\kappa_{\text{inter–M}}(t) = \frac{C_{IM}(t)}{S(t)}, \quad (11)$$

$$\kappa_{\text{intra–M}}(t) = \frac{C_{IC}(t)}{S(t)}. \quad (12)$$

Note that $\kappa_{\text{inter–M}}(t)$ corresponds to the original coupling parameter defined by Cao and Likhtman,[9] who evaluated the cross-correlation between linear polymers. In this respect, $\kappa_{\text{inter–M}}(t)$ is referred as the inter-molecular coupling parameter. Because $\kappa_{\text{intra–M}}(t)$ represents the cross-correlation between different constituent chains in the same molecule, it is referred as the intra-molecular coupling parameter.

RESULTS

Comparison of viscoelasticity with experiments

Figures 1 and 2 show the linear viscoelasticity. The simulation results (curves) are in reasonable agreement with the experimental data (symbols). In the tube theories for branch polymers, a matter of discussion is the so-called hopping parameter p^2 that tunes the frequency of branch point hopping along the backbone.[48] The simulation used in this study is free from the parameter, owing to the branch point dynamics in the dilated network.[41] Nevertheless, the agreement with the data validates the simulation, and it supports further analysis for the correlation functions.

Auto- and cross-correlations

Figure 3 shows the correlation functions $S(t)$, $A_M(t)$. and $A_C(t)$ for the 4- and 6-arm star-branched polymers. As reported for linear polymers earlier,[9–11] there is a clear discrepancy between $S(t)$ (black curves) and $A_M(t)$ (red dotted curves) indicating the significance of $C_{IM}(t)$. As shown later, the contribution of $C_{IM}(t)$ in $S(t)$ is almost identical to that for linear polymers. The difference between $A_M(t)$ and $A_C(t)$ (blue broken curves) is not large. This result indicates that $C_{IC}(t)$ is much smaller than $C_{IM}(t)$, as explicitly shown later.

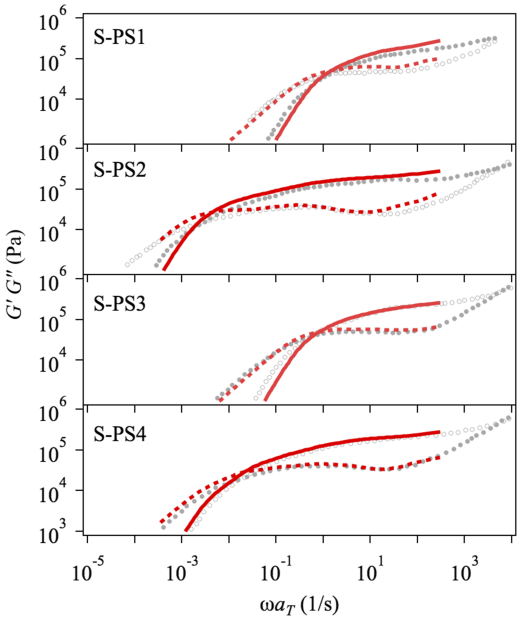

FIG. 1. Linear viscoelasticity for 4- and 6-arm star-branched polystyrene melts at $T = 169.5\,^{\circ}\mathrm{C}$. Filled and unfilled circles are G' and G'' for the experimental data extracted from the literature.[37] Solid and dotted curves are G' and G'' obtained from the simulations.

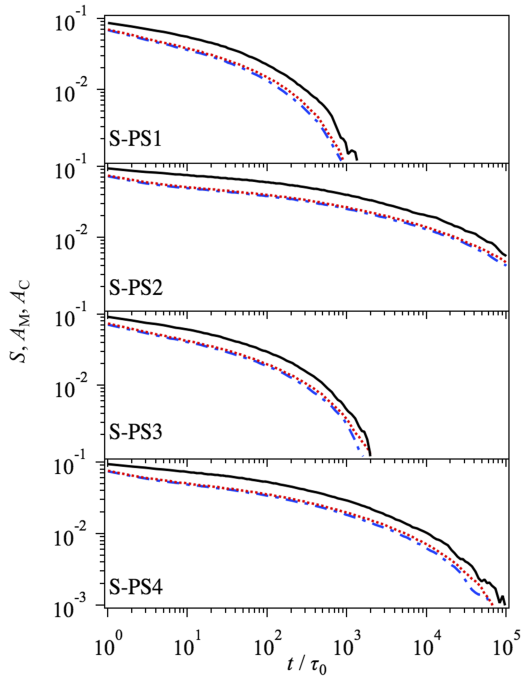

FIG. 3. $S(t)$ (black curve), $A_{\mathrm{M}}(t)$ (red dotted curve), and $A_{\mathrm{C}}(t)$ (blue broken curve) for 4- and 6-arm star-branched polymers.

Figure 4 shows the correlation functions for the H-branched polymers. Interestingly, the difference between $S(t)$ (black curves) and $A_{\mathrm{M}}(t)$ (red dotted curves) is similar to that for the star-branched polymers, as well as for the linear polymer (bottom panel), demonstrating the universality of $C_{\mathrm{IM}}(t)$ contribution to $S(t)$ with respect to the examined long chain branching. On the other hand, the difference between $A_{\mathrm{M}}(t)$ and $A_{\mathrm{C}}(t)$ (blue broken curve) is rather apparent for the H-branched polymers with small molecular weights. This result suggests that $C_{\mathrm{IC}}(t)$ contribution is dependent on branching structures. The auto-correlation function for the constituent chains $A_{\mathrm{C}}(t)$ (blue broken curve) is decomposed into the contributions from the arms and the backbone chains and shown by green curves. The decomposed relaxation functions clearly exhibit the retarded relaxation of the backbone chains (green solid curves) to the arm chains (green dotted curves), as

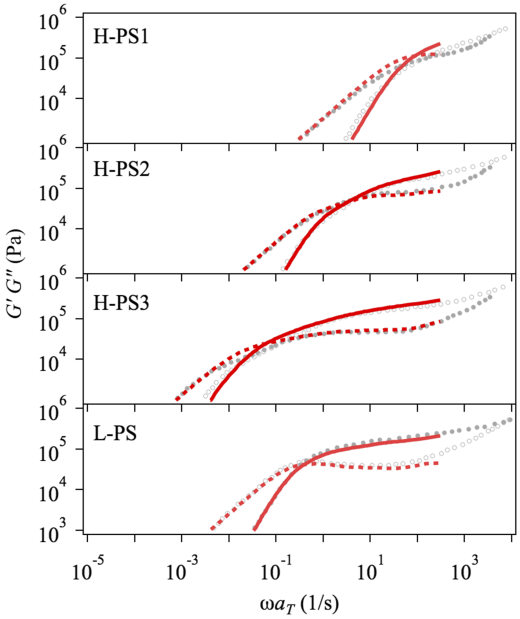

FIG. 2. Linear viscoelasticity for the H-branched and linear polystyrene melts at $T = 169.5\,^{\circ}\mathrm{C}$. Filled and unfilled circles are G' and G'' for the experimental data extracted from the literature.[38] Solid and dotted curves are G' and G'' obtained from the simulations.

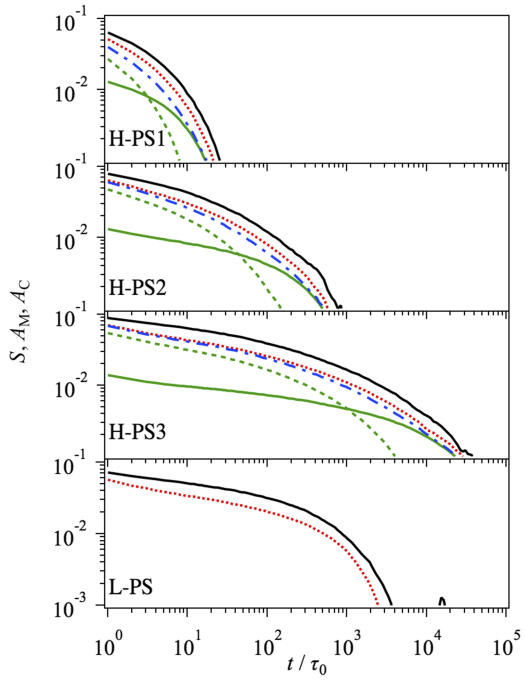

FIG. 4. $S(t)$ (black curve), $A_{\mathrm{M}}(t)$ (red dotted curve), and $A_{\mathrm{C}}(t)$ (blue broken curve) for H-polymers. The contributions from arm and backbone chains in $A_{\mathrm{C}}(t)$ are separately shown by dotted and solid green curves, respectively. $S(t)$ and $A_{\mathrm{M}}(t)$ for the linear polymer are shown in the bottom panel.

expected, although such a two-step behavior is not apparent in $A_C(t)$.

Inter- and intra-molecular coupling parameters

Figure 5 shows the coupling parameters $\kappa_{\text{inter-M}}(t)$ (solid curves) and $\kappa_{\text{intra-M}}(t)$ (broken curves) for the 4- and 6-arm star-branched (top panel) and H-branched (bottom panel) polymers with $\kappa_{\text{inter-M}}(t)$ of the linear polymer (black curve). The results demonstrate that the inter-molecular coupling parameter $\kappa_{\text{inter-M}}(t)$ is virtually universal with respect to the branch structure. Namely, for all the examined cases, $\kappa_{\text{inter-M}}(t)$ curves overlap with each other showing a gradual increase to a steady value around 0.3. Because the time development of $\kappa_{\text{inter-M}}(t)$ is rather mild, and the short time behavior may be concealed by the short time relaxations like glassy behaviors that are not considered in the present simulation, $\kappa_{\text{inter-M}}(t)$ could be fairly regarded as a constant for real systems. This result lends support to the single chain models, in which the inter-molecular coupling is not explicitly considered but implicitly taken account in the stress-optical coefficient. For example, van Ruymbeke *et al.*[30] have reproduced the present dataset of H-branched polystyrenes by their single chain model with a tuning of the plateau modulus.

The intra-molecular coupling parameter $\kappa_{\text{intra-M}}(t)$ shows a few remarkable features, which are different from $\kappa_{\text{inter-M}}(t)$. Apparently, $\kappa_{\text{intra-M}}(t)$ is dependent on the branch structure, and $\kappa_{\text{intra-M}}(t)$ is larger for H-branched polymers than that for the star-branched polymers. This difference is rational due to the hierarchical relaxation mechanism,[27,28,43,46,49] which induces cross-correlations between the arm chain and the backbone chain for H polymers. The other feature of $\kappa_{\text{intra-M}}(t)$ is that it grows with time showing molecular weight dependence. This behavior is related to the entanglements formed between constituent chains composing the same molecule, as discussed later. Nevertheless, the magnitude of $\kappa_{\text{intra-M}}(t)$ is much smaller than that of $\kappa_{\text{inter-M}}(t)$ so that its effect on $S(t)$ is rather limited.

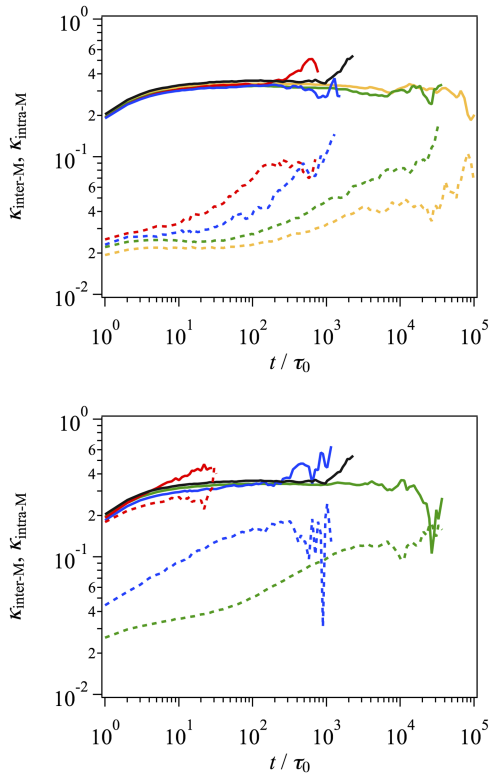

FIG. 5. $\kappa_{\text{inter-M}}(t)$ (solid curves) and $\kappa_{\text{intra-M}}(t)$ (broken curves). Top panel shows the results for 4- and 6-arm star-branched polymers: S-PS1 (red), S-PS2 (orange), S-PS3 (blue), and S-PS4 (green). Bottom panel shows the results for H-branched polymers: H-PS1 (red), H-PS2 (blue), and H-PS3 (green). $\kappa_{\text{IM}}(t)$ for L-PS is indicated by the black solid curve.

DISCUSSION

Effects of intra-molecular and intra-chain entanglements

The complicated behavior of $\kappa_{\text{intra-M}}(t)$ shown in Fig. 5 is related to intra-molecular entanglements, which are formed between constituent chains composing the same molecule. Owing to the model construction,[44] tracing each entanglement (slip-link) in the system is straightforward in the simulations. In this study, the survival probability of slip-links was obtained as the ratio of slip-links that have not disentangled until certain observation time to the total number of slip-links in the system as a whole. Figure 6 shows the survival probability φ thus obtained. It is also straightforward to discriminate the slip-links into those formed between segments in the same molecule (intra-molecular entanglements), and in different molecules (inter-molecular entanglements). The intra-molecular entanglements can be further decomposed into those formed in the same chain (intra-chain entanglements) and between different constituent chains (inter-chain

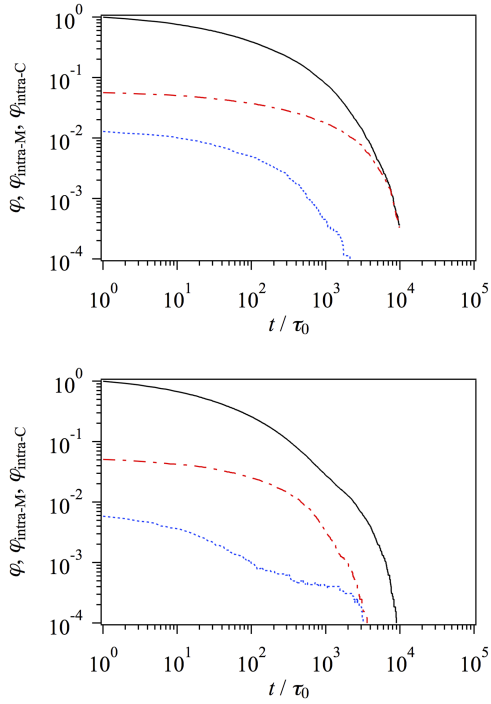

FIG. 6. Survival probability of entanglements for S-PS1 (top) and H-PS2 (bottom). Black, red, and blue curves display the whole entanglements φ, the intra-molecular entanglements $\varphi_{\text{intra-M}}$, and the intra-chain entanglements $\varphi_{\text{intra-C}}$, respectively.

yet intra-molecular entanglements). The survival probability can be obtained for each class of entanglement, and Fig. 6 shows the surviving amount of intra-molecular and intra-chain entanglements normalized by the total number of entanglements, $\varphi_{\text{intra-M}}$ and $\varphi_{\text{intra-C}}$. Although the amounts of intra-molecular and intra-chain entanglements are dependent on the branch structure, for the examined cases, they are not large. In this sense, the effects of such entanglements on the plateau modulus would be negligible for the examined cases.

The kinetics of $\varphi_{\text{intra-M}}$ is dependent on the branching structure. For the case of star polymers (top panel), the intra-molecular entanglements are rather long-lived than the other entanglements. This long-lived behavior of intra-molecular entanglements can be explained in relation to the branch point dynamics. Entanglements formed between different molecules would be released by the translational diffusion of the molecules. In other words, the motion of the branch point contributes the relaxation of inter-molecular entanglements, as reported earlier.[41] On the contrary, the branch point dynamics has no effect on the intra-molecular entanglements, and the disentanglement process is exclusively due to the arm retraction. Nevertheless, the inter-molecular entanglements are long-lived for the star polymers, and consequently, $\varphi_{\text{intra-M}}$ dominates φ as a whole at the terminal region. This $\varphi_{\text{intra-M}}$ behavior appears in $\kappa_{\text{intra-M}}(t)$, which increases over time (see Fig. 5, top panel). The ratio of $\varphi_{\text{intra-M}}$ to φ also increases over time for H-branched polymers (bottom panel), but it saturates at a certain magnitude, as seen in $\kappa_{\text{intra-M}}(t)$ (Fig. 5, bottom panel) that exhibits a plateau. The behavior of $\varphi_{\text{intra-M}}$ for the H-branched polymers would be attributable to the translational diffusion of two branch points in the same molecule, in addition to the arm retraction around each branch point.

Effects of osmotic force

The results shown in Fig. 5, indicating the significance of the inter-molecular cross-correlation term, may suggest the significance of the osmotic force, which suppresses the density fluctuations (see the Appendix for details of the osmotic force). This argument was examined by changing the intensity of the osmotic force. For this sake, additional simulations for S-PS3 were performed with various intensity parameter ε, whereas the segment density was fixed at 10.

Figure 7 shows $\kappa_{\text{inter-M}}(t)$ and $\kappa_{\text{intra-M}}(t)$ with various ε. $\kappa_{\text{inter-M}}(t)$ and $\kappa_{\text{intra-M}}(t)$ are virtually insensitive to ε for $\varepsilon \geq 1.0$, whereas $\kappa_{\text{inter-M}}(t)$ decreases and $\kappa_{\text{intra-M}}(t)$ increases with decreasing ε for $\varepsilon < 1.0$. These results demonstrate that the inter-molecular and intra-molecular cross-correlations are related to the local density fluctuations. For higher ε values, because the osmotic force does not allow large density fluctuations, the molecules move in a correlated manner to maintain homogeneity. On the contrary, for smaller ε values, the molecules can move rather independently. Although this argument is intuitive, it is fair to mention that the osmotic force installed in the present model is completely phenomenological, and its microscopic basis is not clear. Indeed, the osmotic free energy [Eq. (A3)] is defined as a function of the

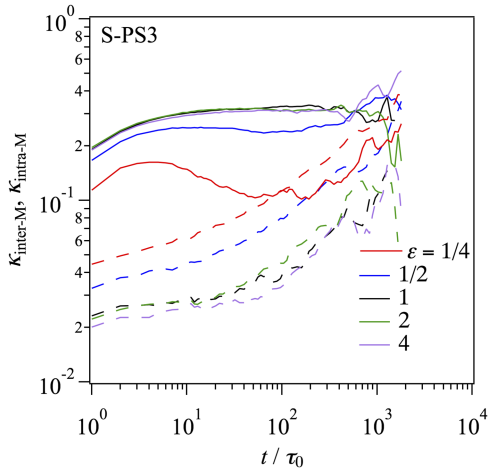

FIG. 7. $\kappa_{\text{inter-M}}(t)$ (solid curves) and $\kappa_{\text{intra-M}}(t)$ (broken curves) for S-PS3 with various ε values.

entanglement segment density, for which incompressibility is not known.

For the results shown in Fig. 7, one may argue that the results in Fig 5 are dependent on the choice of ε. However, for the ε values with which $\kappa_{\text{inter-M}}(t)$ and $\kappa_{\text{intra-M}}(t)$ are ε-dependent, $S(t)$ is not consistent with the experiment. Figure 8 shows the relaxation functions for various ε values. Remind that $S(t)$ for $\varepsilon = 1.0$ is consistent with the experimental $G^*(\omega)$ as shown in Fig. 1. For $\varepsilon > 1.0$, $S(t)$ is not largely disturbed by the change of ε, and thus, the consistency with the experimental data for $G^*(\omega)$ is retained. In contrast, for $\varepsilon < 1.0$, $S(t)$ depends on ε being inconsistent with the experiment. For instance, $S(t)$ at $\varepsilon = 0.5$ (shown by dotted curve) exhibits excess long time relaxation modes. Similar relaxation behavior is seen for $A_{\text{M}}(t)$. These relaxation behaviors are attributable to the inhomogeneity due to large density fluctuations. Figure 9 shows typical snapshots for S-PS3 with $\varepsilon = 0.5$ (left) and $\varepsilon = 1.0$ (right). Apparently, for $\varepsilon = 0.5$, the system exhibits a void formation with strong inhomogeneity. The chain statistics and dynamics under such conditions are

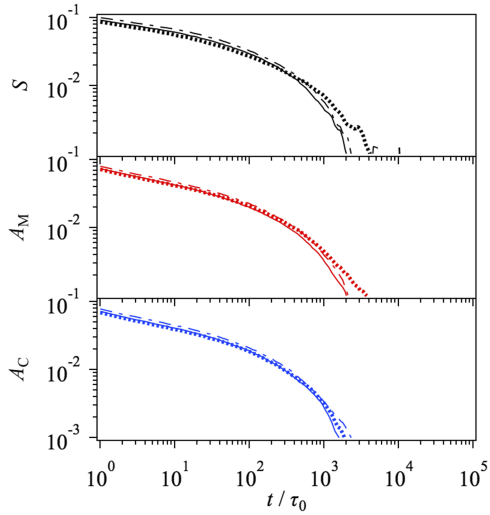

FIG. 8. $S(t)$ (top), $A_{\text{M}}(t)$ (mid), and $A_{\text{C}}(t)$ (bottom) for S-PS3 with various ε values: 1/2 (dotted curve), 1 (solid curve), and 2 (broken curve).

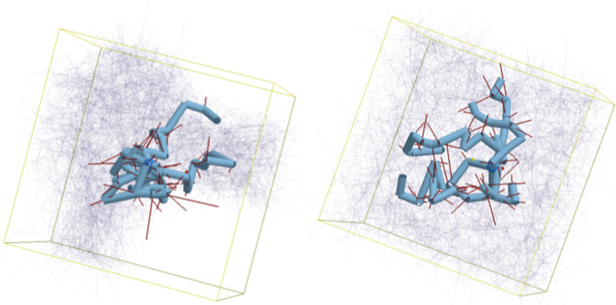

FIG. 9. Typical snapshots of the simulations for S-PS3 with $\varepsilon = 0.5$ (left) and $\varepsilon = 1.0$ (right). One of the molecules is emboldened and the other molecules are shown by thin lines for clarity. Red lines are the entangled segments for the highlighted molecule. The frame in yellow shows the simulation cell for the periodic boundary condition.

different from those under homogeneous situations. Nevertheless, as long as the osmotic force is chosen to prevent inhomogeneity, the relaxation functions are not sensitive to ε.

CONCLUSIONS

The contributions from inter-molecular and intra-molecular orientational cross-correlations (OCC) to the linear relaxation modulus were discussed for the entangled 4- and 6-arm star-branched and H-branched polymers in terms of the multi-chain slip-link simulations. Before the analysis, the simulated linear viscoelastic responses were compared with the literature data for the branched polystyrene melts and reasonable agreement was confirmed. Afterwards, the relaxation modulus was decomposed into self-correlation for the same molecule and cross-correlation between different molecules. The amount of inter-molecular cross-correlation thus obtained was virtually independent of the branching structure and almost identical to that obtained for linear polymers. The simulations with various intensity of the osmotic force suggested that the amount of inter-molecular cross-correlation is affected by the density fluctuations (i.e., incompressibility). The self-correlation for the same molecule was further decomposed into self- and cross-correlations with respect to the constituent chains composing the same molecule. The intra-molecular (yet inter-chain) cross-correlation was strongly dependent on the branch structure, although the contribution was relatively small and almost negligible in comparison to the inter-molecular cross-correlation. This behavior was discussed in terms of entanglements formed between constituent chains in the same molecule.

Although the inter-molecular cross-correlation is not negligible, the results obtained in the present study lend support to the single chain models, in which the cross-correlation is not explicitly considered. The present results demonstrate that the time development of cross-correlation is rather mild. Thus, the effects on the relaxation modulus could be fairly embedded into the stress-optical coefficient in the single chain models. However, the discrimination of the cross-correlation effects from the others such as fluctuations at entanglements is yet to be examined.

Finally, it is fair to note that, as mentioned earlier, the model used in this study is not thermodynamically rigorous, and thus, the obtained results may not be universal for the other models. A possible attack on this issue is to compare the cross-correlations in various multi-chain models. Further studies are being conducted, and the results will be published elsewhere.

ACKNOWLEDGMENTS

The authors thank Professor Alexei Likhtman for his valuable comments on this study. This work is supported in part by Grant-in-Aid for Scientific Research (A) (No. 17H01152) from JSPS and by the Council for Science, Technology and Innovation, Cross-ministerial Strategic Innovation Promotion Program, "Structural Materials for Innovation" from JST.

APPENDIX: OSMOTIC FORCE

In this section, the osmotic force used in the primitive chain network model is described. To suppress density fluctuations, the osmotic force is embedded in the kinetic equations for the slip-link motion and the chain sliding along the primitive path. The equation of motion for the slip-link position $\mathbf{R}$ and the rate equation for the number of Kuhn segments on each entanglement segment n are written as

$$2\zeta\dot{\mathbf{R}} = \sum_{i}^{4} \mathbf{F}_i + \mathbf{F}_\mathbf{f} + \mathbf{F}_\mathbf{B}, \tag{A1}$$

$$\frac{\zeta}{\rho}\dot{n} = (F_i - F_{i-1}) + f_\mathrm{f} + f_\mathrm{B}. \tag{A2}$$

The left-hand sides of the equations represent the drag force and ζ is the friction coefficient of the segment. Prefactor 2 in Eq. (A1) is due to the fact that two segments are bundled at one slip-link. The first terms on the right-hand sides of the equations are the balance of elastic forces among/between the connected segments. The second terms, $\mathbf{F}_\mathrm{f}$ and f_f, are the osmotic forces. The third terms, $\mathbf{F}_\mathrm{B}$ and f_B, are the random forces representing thermal agitations.

The osmotic forces are derived from the phenomenological free energy written in the normalized form as

$$A(\mathbf{R}) = \begin{cases} \dfrac{\varepsilon}{2}\left(\dfrac{\phi(\mathbf{R})}{\langle\phi\rangle} - 1\right)^2 & \text{for } \phi(\mathbf{R}) > \langle\phi\rangle \\ 0 & \text{for } \phi(\mathbf{R}) \le \langle\phi\rangle \end{cases}. \tag{A3}$$

Here, ϕ is the local segment density and $\langle\phi\rangle$ is its average value for the whole system. The phenomenological parameter ε determines the intensity of the osmotic forces. In the simulation, although both $\langle\phi\rangle$ and ε are the parameters arbitrarily chosen, $\langle\phi\rangle$ was fixed at 10 and ε were varied for the discussion of the osmotic force in Figs. 7–9. Although these parameters are related to thermodynamic measures of real materials, the relation has been unknown.[31]

[1] Y. Masubuchi, Annu. Rev. Chem. Biomol. Eng. **5**, 11 (2014).
[2] J. A. Kornfield, G. G. Fuller, and D. S. Pearson, Macromolecules **22**, 1334 (1989).
[3] M. Doi, D. Pearson, J. Kornfield, and G. Fuller, Macromolecules **22**, 1488 (1989).
[4] C. M. Ylitalo, J. A. Kornfield, G. G. Fuller, and D. S. Pearson, Macromolecules **24**, 749 (1991).

[5]R. Graf, A. Heuer, and H. W. Spiess, Phys. Rev. Lett. **80**, 5738 (1998).
[6]J. Gao and J. H. Weiner, J. Chem. Phys. **91**, 3168 (1989).
[7]A. E. Likhtman, S. K. Sukumaran, and J. Ramirez, Macromolecules **40**, 6748 (2007).
[8]A. E. Likhtman, J. Non-Newtonian Fluid Mech. **157**, 158 (2009).
[9]J. Cao and A. E. Likhtman, Phys. Rev. Lett. **104**, 207801 (2010).
[10]Y. Masubuchi and S. K. Sukumaran, Nihon Reoroji Gakkaishi **41**, 1 (2013).
[11]Y. Masubuchi and Y. Amamoto, Nihon Reoroji Gakkaishi **44**, 219 (2016).
[12]Y. Masubuchi and Y. Amamoto, Macromolecules **49**, 9258 (2016).
[13]Y. Masubuchi, Y. Amamoto, A. Pandey, and C.-Y. Liu, Soft Matter **13**, 6585 (2017).
[14]Y. Masubuchi, A. Pandey, and Y. Amamoto, J. Soc. Rheol., Jpn. **45**, 175 (2017).
[15]M. Doi and S. F. Edwards, *The Theory of Polymer Dynamics* (Clarendon Press, Oxford, 1986).
[16]S. T. Milner and T. C. B. McLeish, Phys. Rev. Lett. **81**, 725 (1998).
[17]A. E. Likhtman and T. C. B. McLeish, Macromolecules **35**, 6332 (2002).
[18]E. van Ruymbeke, R. Keunings, and C. Bailly, J. Non-Newtonian Fluid Mech. **128**, 7 (2005).
[19]C. C. Hua and J. Schieber, J. Chem. Phys. **109**, 10018 (1998).
[20]R. N. Khaliullin and J. D. Schieber, Macromolecules **42**, 7504 (2009).
[21]R. G. Larson, T. Sridhar, L. G. Leal, G. H. McKinley, A. E. Likhtman, and T. C. B. McLeish, J. Rheol. **47**, 809 (2003).
[22]E. van Ruymbeke, D. Vlassopoulos, M. Kapnistos, C. Y. Liu, and C. Bailly, Macromolecules **43**, 525 (2010).
[23]R. Everaers, Phys. Rev. E **86**, 1 (2012).
[24]Y. Masubuchi, G. Ianniruberto, F. Greco, and G. Marrucci, J. Chem. Phys. **119**, 6925 (2003).
[25]S. T. Milner and T. C. B. McLeish, Macromolecules **30**, 2159 (1997).
[26]R. C. Ball and T. McLeish, Macromolecules **22**, 1911 (1989).
[27]T. C. B. McLeish, Europhys. Lett. **6**, 511 (1988).
[28]R. G. Larson, Macromolecules **34**, 4556 (2001).
[29]C. Das, N. J. Inkson, D. J. Read, M. A. Kelmanson, and T. C. B. McLeish, J. Rheol. **50**, 207 (2006).
[30]E. van Ruymbeke, C. Bailly, R. Keunings, and D. Vlassopoulos, Macromolecules **39**, 6248 (2006).
[31]T. Uneyama and Y. Masubuchi, J. Chem. Phys. **135**, 184904 (2011).
[32]Y. Masubuchi, T. Uneyama, H. Watanabe, G. Ianniruberto, F. Greco, and G. Marrucci, J. Chem. Phys. **132**, 1 (2010).
[33]T. Uneyama and Y. Masubuchi, J. Chem. Phys. **137**, 154902 (2012).
[34]V. C. Chappa, D. C. Morse, A. Zippelius, and M. Müller, Phys. Rev. Lett. **109**, 148302 (2012).
[35]A. Ramírez-Hernández, F. A. Detcheverry, B. L. Peters, V. C. Chappa, K. S. Schweizer, M. Müller, and J. J. de Pablo, Macromolecules **46**, 6287 (2013).
[36]M. Langeloth, Y. Masubuchi, M. C. Böhm, and F. Müller-plathe, J. Chem. Phys. **138**, 104907 (2013).
[37]W. W. Graessley and J. Roovers, Macromolecules **12**, 959 (1979).
[38]J. Roovers, Macromolecules **17**, 1196 (1984).
[39]Y. Masubuchi, H. Watanabe, G. Ianniruberto, F. Greco, and G. Marrucci, Macromolecules **41**, 8275 (2008).
[40]Y. Masubuchi, G. Ianniruberto, F. Greco, and G. Marrucci, J. Non-Newtonian Fluid Mech. **149**, 87 (2008).
[41]Y. Masubuchi, T. Yaoita, Y. Matsumiya, and H. Watanabe, J. Chem. Phys. **134**, 194905 (2011).
[42]Y. Masubuchi, Y. Matsumiya, H. Watanabe, S. Shiromoto, M. Tsutsubuchi, and Y. Togawa, Rheol. Acta **51**, 1 (2012).
[43]Y. Masubuchi, Y. Matsumiya, H. Watanabe, G. Marrucci, and G. Ianniruberto, Macromolecules **47**, 3511 (2014).
[44]Y. Masubuchi, J.-I. I. Takimoto, K. Koyama, G. Ianniruberto, G. Marrucci, and F. Greco, J. Chem. Phys. **115**, 4387 (2001).
[45]Y. Masubuchi, G. Ianniruberto, F. Greco, and G. Marrucci, Modell. Simul. Mater. Sci. Eng. **12**, S91 (2004).
[46]Y. Masubuchi, G. Ianniruberto, F. Greco, and G. Marrucci, Rheol. Acta **46**, 297 (2006).
[47]T. C. B. McLeish and R. G. Larson, J. Rheol. **42**, 81 (1998).
[48]T. C. B. McLeish, J. Allgaier, D. K. Bick, G. Bishko, P. Biswas, R. Blackwell, B. Blottiere, N. Clarke, B. Gibbs, D. J. Groves, A. Hakiki, R. K. Heenan, J. M. Johnson, R. Kant, D. J. Read, and R. N. Young, Macromolecules **32**, 6734 (1999).
[49]T. C. B. McLeish, Macromolecules **21**, 1062 (1988).